Heterogeneous & Homogeneous & Bio-

CHEMCATCHEM

CATALYSIS

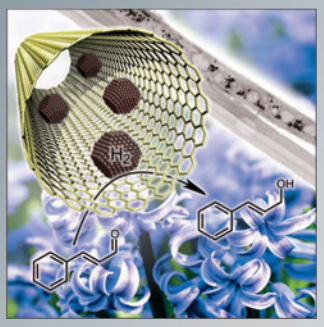

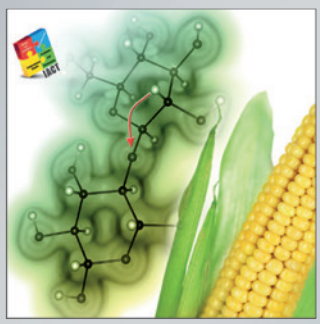

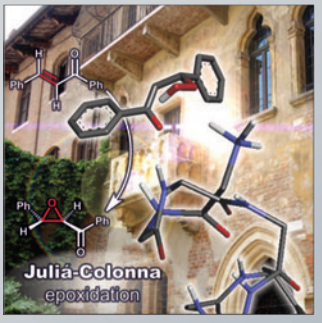

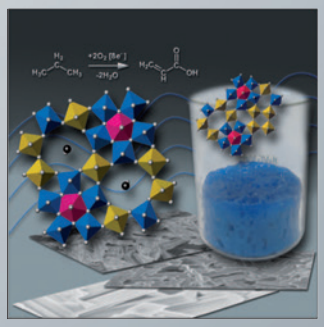

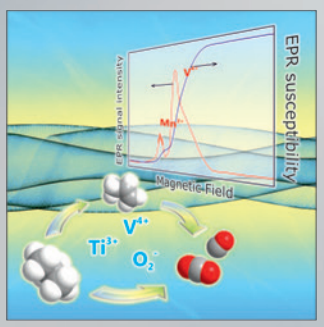

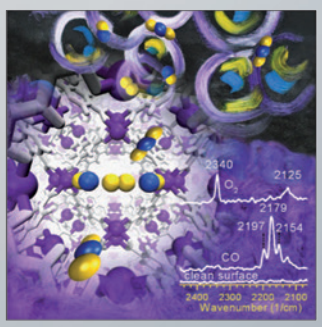

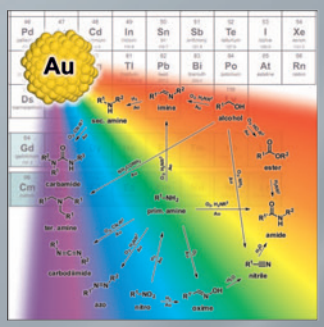

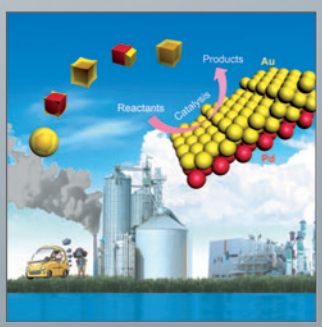

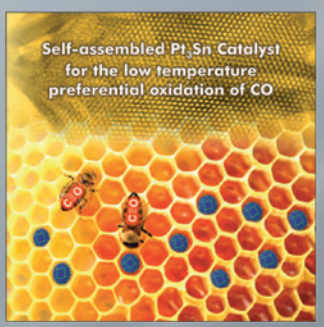

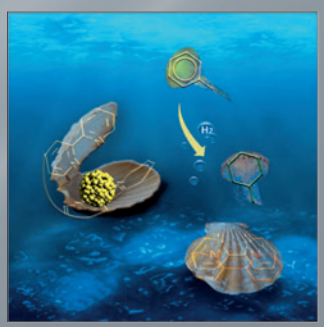

Reprint

A Journal of

ChemPubSoc Europe

WILEY-VCH

www.chemcatchem.org

ChemPubSoc Europe

DOI: 10.1002/cctc.201901847

CHEMCATCHEM Communications

New Role of Pd Hydride as a Sensor of Surface Pd Distributions in Pd–Au Catalysts

Erjia Guan,[a] Alexandre C. Foucher,[b] Nicholas Marcella,[a] Tanya Shirman,[c, d] Mathilde Luneau,[e] Ashley R. Head,[f] David M. A. Verbart,[e] Joanna Aizenberg,[c, d, e] Cynthia M. Friend,[c, e] Dario Stacchiola,[f] Eric A. Stach,[b] and Anatoly I. Frenkel*[a, g]

Isolated or contiguous, the surface distributions of Pd atoms in the Pd–Au bimetallic nanoparticle (NP) catalysts often influence activity and selectivity towards specific reactions. In this study, we used a concomitant Pd hydride formation upon H_2 exposure as a probe of presence of contiguous Pd regions in bimetallic NPs. For demonstrating this method, we prepared silica supported monometallic Pd and bimetallic Pd–Au NPs with a Pd/Au ratio of 25/75 ($Pd_{25}Au_{75}$) and used X-ray absorption spectroscopy, scanning transmission electron microscopy and infrared spectroscopy to detect and quantitatively analyze the Pd hydride regions. This work provides a new approach to characterizing intra-particle heterogeneities within the bimetallic NPs at ambient temperature and pressure.

Pd–Au bimetallic catalysts have been intensively studied because they often exhibit enhanced activity, selectivity and stability, compared with the monometallic Pd or Au catalysts. Examples include their superior activity and/or selectivity towards low-temperature CO oxidation,[1] synthesis of vinyl acetate,[2] selective hydrogenation of hydrocarbons,[3] direct H_2O_2 synthesis from H_2 and O_2,[4] and a number of other reactions. Although Pd and Au are miscible in almost all compositions,[5] the different surface free energies and lattice mismatch between bulk (or nanoscale) Au and Pd often lead to intra-particle compositional and structural heterogeneities that can range from Au-core-Pd-shell[6] to Pd-core-Au-shell[7] structure in Pd–Au nanoparticles, in addition to reports of their quasi-homogeneous mixing[1b,8] in broad compositional ranges. The surface distribution of Pd atoms in Pd–Au particles significantly influences the performance of the catalysts, e.g. isolated Pd sites on surface facilitate vinyl acetate[9] and hydrogen peroxide formation,[10] while contiguous Pd sites are essential for O_2 dissociation[11] and N_2O decomposition.[12] However, characterizing the surface distribution of Pd sites within Pd–Au particles is challenging for samples with dilute Pd or Au compositions, and characterizations generally require non-ambient conditions. For example, cryogenic conditions are required when using CO as a probe molecule in infrared spectroscopy to avoid CO induced restructuring of Pd–Au catalysts[11] and vacuum conditions are required for sensitive surface science techniques. Either cryogenic or UHV condition limits the methods for in-situ/operando characterizations of the catalysts.

In this study, we have taken advantage of the known sensitivity of Pd nanoparticles to form Pd hydrides under hydrogen exposure as a sensor for Pd distributions within the Pd–Au catalysts.[13] Pd hydride formation can only occur on contiguous Pd atom assemblies near the surface within the Pd–Au NPs and can be tracked by the Pd–Pd bond expansion upon hydrogen absorption in X-ray absorption spectroscopy (XAS).[13a] XAS detection of Pd hydride formation in the alloy open new opportunities for catalysis research, due to the high penetration depth of hard X-rays and the compatibility of XAS technique with operando characterization requirements. To demonstrate this method, we prepared silica supported monometallic Pd nanoparticles (Pd NPs) and Pd–Au nanoparticles with a Pd/Au ratio of 25/75 ($Pd_{25}Au_{75}$ NPs) and exposed the samples to hydrogen at ambient pressure and temperature. The structure of the NPs was characterized by a combination of electron microscopy, XAS and infrared (IR) spectroscopy.

Silica supported Pd NPs and $Pd_{25}Au_{75}$ NPs were synthesized by modified literature procedures (details in the SI).[14] The

[a] Dr. E. Guan, N. Marcella, Prof. A. I. Frenkel
Department of Materials Science and Chemical Engineering
Stony Brook University
Stony Brook NY-11794 (USA)
E-mail: anatoly.frenkel@stonybrook.edu
[b] A. C. Foucher, Prof. E. A. Stach
Materials Science and Engineering
University of Pennsylvania
Philadelphia PA-19104 (USA)
[c] Dr. T. Shirman, Prof. J. Aizenberg, Prof. C. M. Friend
John A. Paulson School of Engineering and Applied Sciences
Harvard University
Cambridge MA-02138 (USA)
[d] Dr. T. Shirman, Prof. J. Aizenberg
Wyss Institute for Biologically Inspired Engineering
Harvard University
Cambridge MA-02138 (USA
[e] Dr. M. Luneau, D. M. A. Verbart, Prof. J. Aizenberg, Prof. C. M. Friend
Department of Chemistry and Chemical Biology
Harvard University
Cambridge MA-02138 (USA)
[f] Dr. A. R. Head, Dr. D. Stacchiola
Center for Functional Nanomaterials
Brookhaven National Laboratory
Upton NY-11973 (USA)
[g] Prof. A. I. Frenkel
Chemistry Division
Brookhaven National Laboratory
Upton NY-11973 (USA)

Supporting information for this article is available on the WWW under https://doi.org/10.1002/cctc.201901847

This publication is part of a Special Collection on "Advanced Microscopy and Spectroscopy for Catalysis". Please check the ChemCatChem homepage for more articles in the collection.

$Pd_{25}Au_{75}$ particles were uniformly distributed in the silica matrix with an average particle size of 6.1 ± 1.9 nm, as evidenced by scanning transmission electron microscopy (STEM) (Figure S1 in the SI). The atomic fraction of Pd in the bimetallic Pd–Au NPs was determined by inductively coupled plasma mass spectrometry (ICP–MS), showing a Pd/Au atomic ratio of, approximately, 25/75.

Energy dispersive X-ray spectroscopy (EDS) on fresh $Pd_{25}Au_{75}$ NPs shows that most of Pd is uniformly distributed within a particle (Figure 1A). However, some particles display small clusters of Pd at the edges with a typical size in the range of 1 nm to 5 nm (Figure 1B). The EDS analysis of $Pd_{25}Au_{75}$ particles after a 2-hour treatment under H_2 at 400 °C also shows the formation of Pd clusters within the particles.

X-ray absorption near-edge structure (XANES) at Pd K-edge showed that Pd is in the form of Pd oxides in the as-prepared silica supported Pd NPs (Figure S2A). A complete reduction of Pd oxides was observed as the catalysts were treated in flowing H_2 (20 mL/min) at 573 K for 30 min (Figure S2B). In contrast, Pd is in near metallic form in the as-prepared silica supported $Pd_{25}Au_{75}$ NPs (Figure S2C). These results are in agreement with previous studies,[15] showing that the Pd–Au alloy phases are more resistant to oxidation than pure Pd during the calcination in catalyst preparations. In order to compare metallic Pd regions, Pd NPs mentioned in the following results are all after fully reduction under H_2 at 573 K for 30 min.

We used X-ray absorption spectroscopy at Pd K-edge as a probe to detect the formation of Pd hydride at room temperature in both monometallic Pd and $Pd_{25}Au_{75}$ NPs on RCT SiO_2. After exposing Pd NPs to flowing H_2 at 298 K and 1 bar, a significant shift was observed in XANES (Figure S3A) and *k*-space EXAFS spectra (Figure S3B) – an effect of Pd hydride formation that has been previously reported.[13a] Correspondingly, the *R*-space EXAFS spectrum of the Pd NPs shifted to longer Pd–Pd distance upon H_2 exposure (Figure 2A). For $Pd_{25}Au_{75}$ NPs upon exposure to flowing H_2, it was difficult to state conclusively whether the spectrum exhibited any shift in the XANES (Figure S4A) due to alloying with Au affecting the sensitivity of XANES to detecting hydride formation and *k*-space EXAFS spectra (Figure S4B), but the spectral changes in *R*-space (Figure 2B) were observed and qualitatively showed structural changes of Pd regions in $Pd_{25}Au_{75}$ NPs under H_2. The H_2–He exposure cycles were repeated for Pd NPs under same conditions and the spectra showed identical shifts under each cycle (Figure S5).

EXAFS data were quantitatively analyzed to characterize the coordination environment of Pd in both Pd NPs and $Pd_{25}Au_{75}$ NPs on RCT SiO_2 under flowing He and H_2 at 298 K and 1 bar (Table 1). Before the test, the Pd NPs were pretreated by H_2 at 573 K for 30 min, followed by a He purge, to fully reduce Pd to metallic form. In Pd NPs under He, the coordination number (CN) of first shell Pd–Pd contribution is approximately 9.2 ± 0.6 at a distance of 2.737 ± 0.003 Å. For such a coordination number, a corresponding size of a supported cuboctahedral nanoparticle would be expected to be between 2 and 3 nm, depending on its shape[13a] in agreement with the average particle sizes of 3.4 ± 1.7 nm obtained by STEM (Figure S6). In $Pd_{25}Au_{75}$ NPs under He, the CNs of Pd–Pd and Pd–Au contributions are 1.1 ± 0.2 and 9.6 ± 0.4, respectively, showing that, on average, Pd atoms are predominantly surrounded by Au atoms, in a greater ratio (9.6:1.1) than that predicted from the bulk composition (3:1). The total CN of Pd-metal (M) is lower than 12 of the bulk, showing that some Pd atoms are on the surface of the NPs and are thus not fully coordinated. The

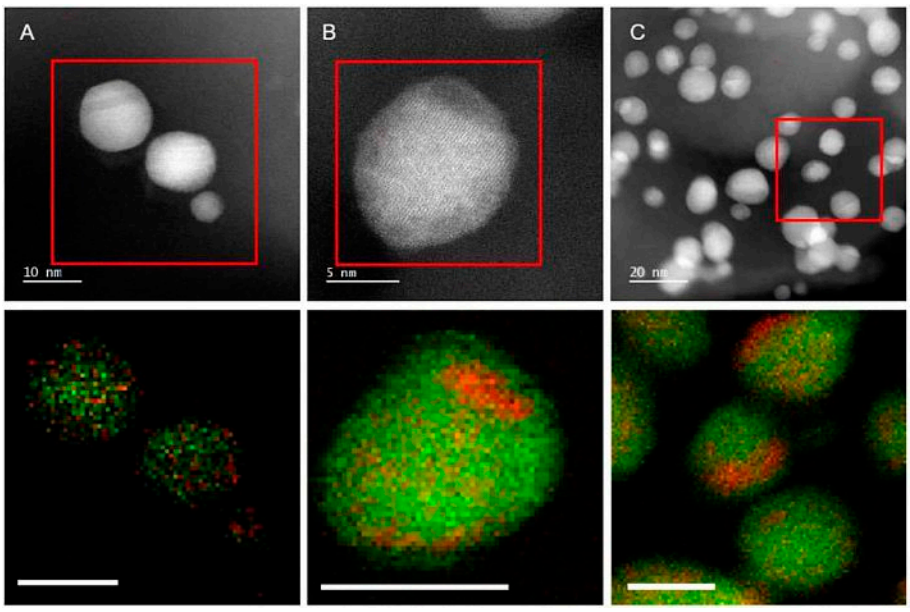

Figure 1. STEM-EDS of $Pd_{25}Au_{75}$ NPs on RCT SiO_2. Pd is in red, Au is in green. The scale bar on the EDS maps represents 10 nm. (A) Selected particles where Pd is uniformly distributed in a particle before H_2 treatment; (B) selected particle where Pd is not uniformly distributed in a particle before H_2 treatment; (C) uniform and non-uniform distribution of Pd within particles after 2 hours of exposure to hydrogen at 400 °C.

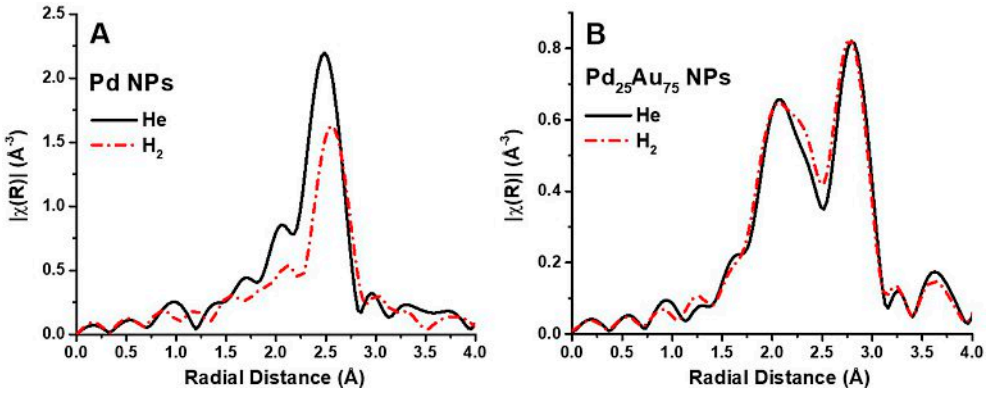

Figure 2. Fourier transform magnitudes of k^2-weighted EXAFS spectra of (A) Pd NPs and (B) $Pd_{25}Au_{75}$ NPs on RCT silica under flowing He or H_2 at 298 K and 1 bar.

Table 1. EXAFS structure parameters representing silica supported Pd and $Pd_{25}Au_{75}$ nanoparticles.[a]

Sample	CN (Pd–Au)	CN (Pd–Pd)	R (Pd–Au) [Å]	R (Pd–Pd) [Å]	σ^2 (Pd–Au) [Å^2]	σ^2 (Pd—Pd) [Å^2]
	–	9.2(6)	–	2.737(3)	–	0.006(1)
Pd (H_2)	–	9.0(6)	–	2.810(3)	–	0.007(1)
$Pd_{25}Au_{75}$ (He)	9.6(4)	1.1(2)	2.811(3)	2.787(8)	0.006(4)	0.003(1)
$Pd_{25}Au_{75}$ (H_2)	9.6(4)	0.9(2)	2.811(3)	2.806(8)	0.006(4)	0.002(1)

[a] *CN*, coordination number; *R*, distance between absorber and backscatterer atoms; σ^2, disorder term (EXAFS Debye-Waller factor). *k*-range: 3.0–13.3 Å^{-1}, *R*-range: 1.4–3.3 Å.

Pd–Pd and Pd–Au distances are 2.787 ± 0.008 Å and 2.811 ± 0.003 Å, respectively, which are between the metal–metal distances of pure NP Pd (2.74 Å, Table 1) and pure NP Au of similar average size (2.88 Å),[16] showing the majority of Pd are in Pd–Au alloy phase in $Pd_{25}Au_{75}$ NPs.

After being exposed to flowing H_2, Pd NPs showed an increase in the Pd–Pd bond distance from 2.737 ± 0.003 Å to 2.810 ± 0.003 Å, which is typical for the lattice expansion from Pd to Pd hydride in NPs.[13a] In the earlier work it was shown that an empirical relationship (1) between the Pd–Pd bond length change ΔR and the H/Pd ratio *x*, known for bulk Pd, can also apply to describe nanoscale Pd[13a] [Equation (1)]:

$$\frac{\Delta R}{R} = 0.0666x - 0.0164x^2 \quad (1)$$

In the Pd NPs, H/Pd ratio calculated using the EXAFS analysis results was found to be 0.45, which is consistent with the value obtained earlier for Pd NPs of similar sizes.[13a] For $Pd_{25}Au_{75}$ NPs, EXAFS analysis also demonstrated that Pd–Pd bond increased from 2.787 ± 0.008 Å to 2.806 ± 0.008 Å. The H/Pd ratio is 0.10 in $Pd_{25}Au_{75}$ NPs upon H_2 exposure, significantly lower than that of Pd NPs, because only contiguous Pd regions on the NPs surface can respond to H_2 and form Pd hydride. Based on the calculated H/Pd ratio, and assuming that all Pd atoms segregate into identically sized regions within $Pd_{25}Au_{75}$ NPs, these Pd region size can be estimated to be of the order of 1 nm. It is the lower bound for the average size of Pd regions, because a subset of randomly distributed Pd atoms will also contribute to the experimentally measured Pd–Pd distance, effectively lowering it with respect to the idealized model described above. This result is consistent with the majority of Pd being in Pd–Au alloy phase in $Pd_{25}Au_{75}$ NPs and provides a sensitive detection for small Pd rich regions within the particles, as evidenced by STEM-EDS (Figure 1). The details of the EXAFS fittings are shown in Figure S7 and S8 in the SI.

EXAFS results showed the formation of Pd hydride in Pd rich regions in the surface of $Pd_{25}Au_{75}$ NPs under H_2. To corroborate these results, we used CO adsorption and IR spectroscopy to probe such metal regions under cryogenic conditions. Pd and $Pd_{25}Au_{75}$ NPs on RCT SiO_2 were first being treated by H_2 at 573 K for 30 min to reduce Pd into metallic form and clean the surface species. The reduced samples were cooled by liquid nitrogen under vacuum conditions and were exposed to CO from 10^{-3} to 10 Torr at 173 K (Figure 3). Monometallic Pd NPs showed ν_{CO} frequencies representing atop CO on Pd (111) and (100) facets/bridging CO at particle edges at 2036 and 1995 cm^{-1}, bridging CO on Pd (111) hollow sites at 1885 cm^{-1}.[17] In $Pd_{25}Au_{75}$ NPs, atop CO on Au was observed at 2103 cm^{-1} at CO pressure as low as 10^{-3} Torr at 173 K. Two atop CO on Pd at 2029 and 2003 cm^{-1}, two weak bridging CO on Au and Pd at 1932 and 1783 cm^{-1} were observed,[18] showing Pd atoms form contiguous Pd islands on the surface of Au NPs and exposing certain facets, mainly (111) and (100).

The method of using hydrogen as a probe improved the sensitivity of X-ray absorption spectroscopy – traditionally considered a bulk technique – in detecting local heterogeneities within the bimetallic NPs. By combining the spectroscopy

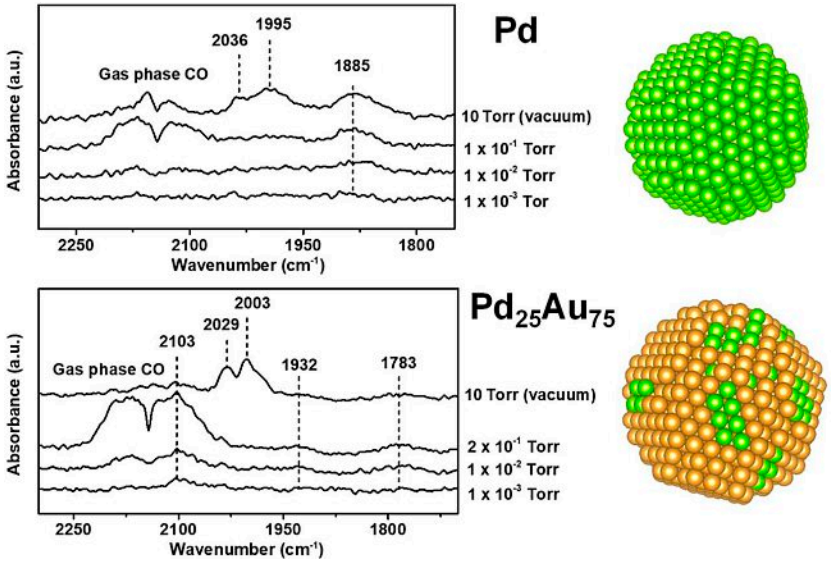

Figure 3. IR spectroscopy characterizing v_{CO} region of reduced Pd nanoparticles and $Pd_{25}Au_{75}$ NPs on RCT SiO_2 at 173 K during exposure to 10^{-3}, 10^{-2}, 10^{-1} and 10 Torr CO, respectively. CO gas was evacuated prior to taking spectra after 10 Torr exposure. The bands at 2173 and 2108 cm^{-1} are v_{CO} of gas phase CO. The simplified models represented Pd and $Pd_{25}Au_{75}$ NPs exposing mainly (111) and (100) facets.

evidence with the observation of Pd rich regions within the NPs using STEM-EDS, we were able to confirm and analyze contiguous Pd regions in supported Pd–Au NPs under ambient pressure and temperature. XAS data at Au L_3 edge are not expected to be sensitive to Pd rearrangement in Pd–Au particles with size of 6.1 nm and relatively low Pd concentration used in this study, but they would be beneficial for Pd–Au catalysts with smaller sizes (1–3 nm) where Pd-hydride formation would be expected to perturb Au atoms stronger. H_2 can be used as an *in-situ* probe in many hydrogenation reactions. For reactions when H_2 is not a reactant, H_2 can be used prior to (or after) the reaction for the determination of heterogeneities of the Pd–Au catalysts. The benefits of using H_2 in the *in-situ* XAS experiment to probe the surface heterogeneities of Pd–Au catalysts may extend to other Pd-containing bimetallic catalysts, such as Pd–Ag catalysts, which attract broad attention for their catalytic performance,[19] but have too small Z-contrast between Pd and Ag to be distinguished by EXAFS and STEM.

Experimental Section

Transmission Electron Microscopy

The $Pd_{25}Au_{75}$ on RCT SiO_2 system was analyzed using a JEOL NEOARM transmission microscope operating at 200 kV. High-resolution EDS analysis was performed on a couple of particles, before and after a 2-hour H_2 treatment at 400 °C with 80% nitrogen and 20% hydrogen. The total flow rate was 50 mL/min.

Infrared Spectroscopy

IR spectra of solid samples were recorded with a Bruker Vertex 80 V FT-IR spectrometer in transmission mode. The samples were pressed into a tungsten mesh and were loaded into a high vacuum IR chamber for data collection. The samples were cooled by liquid nitrogen to around 173 K. CO (Airgas, 99%) was introduced into the chamber with certain pressures (10^{-5} to 10 Torr) measured by a pressure gauge. 256 scans were accumulated for each spectrum (resolution 4 cm^{-1}).

X-Ray Absorption Spectroscopy and Data Analysis

X-ray absorption spectra were recorded in fluorescence mode under flowing He or H_2 at 298 K, 1 atm. Analysis of the EXAFS data was carried out with the software ATHENA and ARTEMIS of the IFEFFIT package. Fifteen spectra were merged after alignment. Amplitude reduction factors S_0^2 (0.87 ± 0.02) were obtained from the EXAFS data fits for Pd foil spectrum and fixed to those values for the determination of coordination numbers in the NPs. Values of the inner potential correction $\triangle E_0$ were fixed for each absorber-backscatterer contribution as 7.9 ± 0.4 eV for Pd NPs and -5.6 ± 0.5 eV for $Pd_{25}Au_{75}$ NPs.

Acknowledgements

The work was supported as part of the Integrated Mesoscale Architectures for Sustainable Catalysis (IMASC), an Energy Frontier Research Center funded by the U.S. Department of Energy (DOE), Office of Science, Basic Energy Sciences under Award No. DE-SC0012573. This research used 8-ID (ISS) beamline of the National Synchrotron Light Source, a U.S. DOE Office of Science User Facility operated for the DOE Office of Science by Brookhaven National Laboratory (BNL) under Contract No. DE-SC0012704. TEM was performed at the Singh Center for Nanotechnology at the University of Pennsylvania, a member of the National Nanotechnology Coordinated Infrastructure (NNCI) network, which is supported by the National Science Foundation (Grant NNCI-1542153). These facilities were also supported in part by the NSF

through the University of Pennsylvania Materials Research Science and Engineering Center (MRSEC) (DMR-1720530). This research used resources of the Center for Functional Nanomaterials, which is a U.S. DOE Office of Science Facility, at BNL under Contract No. DE-SC0012704.

Conflict of Interest

The authors declare no conflict of interest.

Keywords: Bimetallic catalysts · X-ray absorption spectroscopy · Pd–Au nanoparticles · Surface heterogeneity · Pd hydride

[1] a) J. Xu, T. White, P. Li, C. H. He, J. G. Yu, W. K. Yuan, Y. F. Han, *J. Am. Chem. Soc.* **2010**, *132*, 10398–10406; b) M. Luneau, T. Shirman, A. Filie, J. Timoshenko, W. Chen, A. Trimpalis, M. Flytzani-Stephanopoulos, E. Kaxiras, A. I. Frenkel, J. Aizenberg, *Chem. Mater.* **2019**, *31*, 5759–5768.
[2] Y. F. Han, J. H. Wang, D. Kumar, Z. Yan, D. W. Goodman, *J. Catal.* **2005**, *232*, 467–475.
[3] N. El Kolli, L. Delannoy, C. Louis, *J. Catal.* **2013**, *297*, 79–92.
[4] J. K. Edwards, E. Ntainjua N, A. F. Carley, A. A. Herzing, C. J. Kiely, G. J. Hutchings, *Angew. Chem. Int. Ed.* **2009**, *48*, 8512–8515; *Angew. Chem.* **2009**, *121*, 8664–8667.
[5] T. A. Silva, E. Teixeira-Neto, N. López, L. M. Rossi, *Sci. Rep.* **2014**, *4*, 5766.
[6] a) M. Hosseini, T. Barakat, R. Cousin, A. Aboukaïs, B.-L. Su, G. De Weireld, S. Siffert, *Appl. Catal. B* **2012**, *111*, 218–224; b) M. R. Knecht, M. G. Weir, A. I. Frenkel, R. M. Crooks, *Chem. Mater.* **2008**, *20*, 1019–1028.
[7] C. Kan, W. Cai, C. Li, L. Zhang, H. Hofmeister, *J. Phys. D* **2003**, *36*, 1609.
[8] N. A. Merrill, E. M. McKee, K. C. Merino, L. F. Drummy, S. Lee, B. Reinhart, Y. Ren, A. I. Frenkel, R. R. Naik, N. M. Bedford, *ACS Nano* **2015**, *9*, 11968–11979.
[9] M. S. Chen, K. Luo, T. Wei, Z. Yan, D. Kumar, C. W. Yi, D. W. Goodman, *Catal. Today* **2006**, *117*, 37–45.
[10] L. K. Ouyang, G. J. Da, P. F. Tian, T. Y. Chen, G. D. Liang, J. Xu, Y. F. Han, *J. Catal.* **2014**, *311*, 129–136.
[11] F. Gao, Y. L. Wang, D. W. Goodman, *J. Am. Chem. Soc.* **2009**, *131*, 5734–5736.
[12] X. Wei, X. F. Yang, A. Q. Wang, L. Li, X. Y. Liu, T. Zhang, C. Y. Mou, J. Li, *J. Phys. Chem. C* **2012**, *116*, 6222–6232.
[13] a) J. Wang, Q. Wang, X. Jiang, Z. Liu, W. Yang, A. I. Frenkel, *J. Phys. Chem. C* **2014**, *119*, 854–861; b) R. J. Davis, S. M. Landry, J. A. Horsley, M. Boudart, *Phys. Rev. B* **1989**, *39*, 10580–10583.
[14] T. Shirman, J. Lattimer, M. Luneau, E. Shirman, C. Reece, M. Aizenberg, R. J. Madix, J. Aizenberg, C. M. Friend, *Chem. Eur. J.* **2018**, *24*, 1833–1837.
[15] A. M. Venezia, V. La Parola, G. Deganello, B. Pawelec, J. L. G. Fierro, *J. Catal.* **2003**, *215*, 317–325.
[16] A. I. Frenkel, S. Nemzer, I. Pister, L. Soussan, T. Harris, Y. Sun, M. H. Rafailovich, *J. Chem. Phys.* **2005**, *123*.
[17] a) T. Schalow, B. Brandt, D. E. Starr, M. Laurin, S. K. Shaikhutdinov, S. Schauermann, J. Libuda, H. J. Freund, *Phys. Chem. Chem. Phys.* **2007**, *9*, 1347–1361; b) I. V. Yudanov, R. Sahnoun, K. M. Neyman, N. Rosch, J. Hoffmann, S. Schauermann, V. Johanek, H. Unterhalt, G. Rupprechter, J. Libuda, H. J. Freund, *J. Phys. Chem. B* **2003**, *107*, 255–264.
[18] B. Zhu, G. Thrimurthulu, L. Delannoy, C. Louis, C. Mottet, J. Creuze, B. Legrand, H. Guesmi, *J. Catal.* **2013**, *308*, 272–281.
[19] a) G. X. Pei, X. Y. Liu, A. Q. Wang, A. F. Lee, M. A. Isaacs, L. Li, X. L. Pan, X. F. Yang, X. D. Wang, Z. J. Tai, K. Wilson, T. Zhang, *ACS Catal.* **2015**, *5*, 3717–3725; b) Q. W. Zhang, J. Li, X. X. Liu, Q. M. Zhu, *Appl. Catal. A* **2000**, *197*, 221–228.

Manuscript received: September 29, 2019
Revised manuscript received: October 30, 2019
Accepted manuscript online: November 6, 2019
Version of record online: December 11, 2019